

Adaptive multilevel method for the air bearing problem in hard disk drives

Chung-Jen Lu*, Shean-Son Chiou, Tai-Kuo Wang

Department of Mechanical Engineering, National Taiwan University, No. 1 Roosevelt Rd. Sec. 4, Taipei 10617, Taiwan, ROC

Received 10 May 2002; received in revised form 25 December 2003; accepted 7 January 2004

Abstract

An adaptive grid-generating algorithm is constructed and integrated with the multigrid method to form a numerical scheme that suits slider air-bearing simulation of hard disk drives. The relative truncation error, a by-product of the multigrid method, is used in grid adaptation criteria. Finer meshes are constructed over nodes of the current finest grid where the relative truncation error exceeds a predetermined tolerance. The union of these finer meshes forms a new level of grid, which may not cover the entire domain of the coarse grid underneath. The final grid system thus constructed is composed of levels of uniform grids with decreasing mesh sizes. This composite grid structure incorporates with numerical resolution as needed and efficiency of computation. A shaped rail, negative pressure slider is used to demonstrate the effectiveness of this numerical scheme. Compared with the traditional multigrid method, the proposed adaptive multilevel method can significantly reduce the computation work for achieving the same level of accuracy.

© 2004 Elsevier Ltd. All rights reserved.

Keywords: Gas-lubricated bearings; Numerical analysis; Reynolds equation; Hard disk drives

1. Introduction

Since the introduction of the first magnetic hard disk drive, the head-disk spacing has consistently diminished to meet the demand for higher data storage density. The flying heights of recent sliders are in the range of 20–30 nm or below. Besides the extremely low spacing, it is also desirable to have a constant flying height over the entire disk, a low take-off/landing velocity, and a stiff air bearing. In order to meet these strict performance requirements, air bearings of significant complexity have been proposed [1–3]. New features in air bearing designs include shaped rails, multiple etch depths, and recessed regions. Due to the complicated air-bearing surface topography, the pressure distribution under the slider can only be obtained by numerical methods. Therefore, an efficient slider simulator is an indispensable tool for the slider design.

The pressure distribution between the slider and the disk is governed by the generalized Reynolds equation. Considerable attention has been drawn to the development of efficient and stable numerical schemes for solving the generalized Reynolds equation [4–11]. As the modern air-bearing surface (ABS) becomes increasingly complex, the pressure varies dramatically in the area where the ABS height changes suddenly. In order to have a clear picture of the pressure distribution, a fine grid should be used such that the numerical error is below a given border everywhere. This goal can be achieved by using a uniform grid with small mesh size. However, this approach usually leads to a large number of equations and hence significantly deteriorates the efficiency of the numerical simulator. Furthermore, since high resolution is only required over high pressure-gradient regions, which form a proper subset of the entire domain, it is impractically to employ fine meshes globally. Therefore, it is highly desirable to have a robust adaptive grid generator that concentrates high resolving meshes to the critical parts of the domain.

The adaptive grid generators generally have to fulfill two basic goals. First, they have to supply the

* Corresponding author. Tel.: +886-2-23627686; fax: +886-2-23631755.

E-mail address: cjlu@ntu.edu.tw (C.-J. Lu).

discretization approach with a domain partitioning method capable of adapting the size of the discretization cells locally, and second, they should supply the adaptive simulation approach with a method for the evaluation and control of the discrete approximation errors during simulation. The multigrid method is not only an efficient method for solving nonlinear discrete problems but also provides a cheap and reliable way for estimating the discretization error [12–14]. Therefore, it is nature to incorporate the multigrid method with an adaptive grid selection strategy to form an efficient slider simulator.

Lu [10] developed a slider simulator using an adaptive multigrid scheme. He employed a geometric progression scheme to generate the initial rectangular grid. After the pressure solution is obtained on the initial grid, the grid lines are redistributed so that the grid is more concentrated in areas where the pressure gradient is high. Their adaptive grid generation scheme has two shortcomings. First, because high resolution is achieved by adjusting the positions of grid lines, local modification of a discretization cell implies the modification of all the discretization cells along the grid lines. Hence, unnecessary fine meshes may be introduced to where the pressure is smooth. Second, the number of grid lines of the finest grid is fixed; this may restrict the highest resolution and result in meshes with large aspect ratio. This kind of non-uniform grid may cause lower-order discrete approximation. Wu and Bogy [11] combined the multigrid method with an unstructured adaptive triangular mesh generation scheme to form an efficient slider simulator. The unstructured triangular mesh makes it easy to describe the complex geometry of shaped sliders and provides local refinement only to the critical regions. However, the use of unstructured irregular meshes requires complicated data structures and huge information overheads for the representation and modification of grid structures. It is also difficult to apply some efficient iteration schemes, e.g. line relaxation, on such arbitrary grids.

In this study, we present an efficient numerical method, which is suitable for slider air-bearing simulations, based on the multilevel adaptive technique developed by Brandt [12]. A sequence of uniform rectangular grids is used to achieve non-uniform resolution. This capability can be obtained because various grids (levels) need not all extend over the same domain. Finer levels may be confined to increasingly smaller subdomains, so as to provide higher resolution only where desired. Then the multigrid method is used to solve the discrete problem. Because only uniform grids are used, the adaptive grid structures can be defined in terms of simple and manageable data structures that naturally fit into the multigrid method. Finally, a tri-rail slider is used to demonstrate the efficiency of this method.

2. Discretization of the governing equation

The pressure distribution of gas-lubricated bearings is governed by the classical Reynolds equation. However, due to the low flying height of the slider in current hard disk drives, the classical Reynolds equation, which assumes no-slip and continuous flow, is no longer valid. Several modifications have been proposed based on slip boundary conditions and Boltzmann equation. These correction models can be put into the following non-dimensional steady state generalized Reynolds equation

$$\frac{\partial}{\partial X} \left(QPH^3 \frac{\partial P}{\partial X} - \Lambda_x PH \right) + \frac{\partial}{\partial Y} \left(QPH^3 \frac{\partial P}{\partial Y} - \Lambda_y PH \right) = 0, \quad (1)$$

where $P = p/p_a$ is the dimensionless pressure, $H = h/h_m$ the dimensionless bearing height, $X = x/L$ the dimensionless x -coordinate, and $Y = y/L$ the dimensionless y -coordinate, in which p_a , h_m , and L indicate the ambient pressure, the flying height, and the length of the slider, respectively. $\Lambda_x = 6\mu UL/p_a h_m^2$ and $\Lambda_y = 6\mu VL/p_a h_m^2$ are the bearing numbers in the x - and y -directions, respectively, in which U and V are the x and y velocity components, respectively. Q is the flow factor that assumes different forms depending on the type of correction model used [10].

The control volume method is employed to discretize the generalized Reynolds equation. Integration of Eq. (1) over the control volume as shown in Fig. 1 yields

$$J_e - J_w + J_n - J_s = 0,$$

where J indicates the integrated flux and the lower-case subscript denotes the control surface at which the flux is evaluated. The fluxes crossing the control surfaces can be further represented in terms of the values of clearance and pressure at neighboring grid points using the generalized formulation proposed by Patankar [15]. The final discretization form of the equation at grid point P

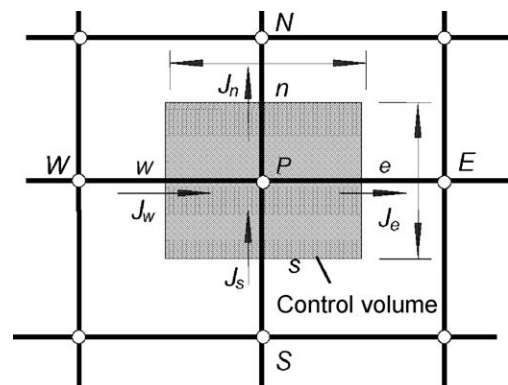


Fig. 1. Illustration of the control volume.

can be written as [10]

$$a_P P_P = a_E P_E + a_W P_W + a_N P_N + a_S P_S + f_P, \quad (2)$$

where the capital subscripts refer to the grid points. Since the coefficients a 's in Eq. (2) are functions of the pressure, the discrete equation is nonlinear.

3. Full approximation storage algorithm

The discretized system of equations can be expressed in the matrix form

$$\mathbf{L}_h \mathbf{u}_h = \mathbf{f}_h, \quad (3)$$

where \mathbf{L}_h is the coefficient matrix formed by the coefficients $a_P, a_E, a_W, a_N,$ and a_S, \mathbf{u}_h the vector of pressure on all grid points, \mathbf{f}_h the source vector. Note that the coefficient matrix, pressure vector, and source vector all depend on the mesh size h . In this paper, the full approximation storage (FAS) algorithm in Brandt [12], which is well suited for nonlinear equations, is employed for solving Eq. (3). The key idea of the FAS algorithm can be understood by considering the case that only two levels of grid are used. The mesh sizes of the fine and coarse grids are h and H , respectively. A suitable iteration method is used on the fine grid to find an approximate solution $\hat{\mathbf{u}}_h$ to Eq. (3). Then the algebraic error in $\hat{\mathbf{u}}_h$ or the correction is

$$\hat{\mathbf{e}}_h = \mathbf{u}_h - \hat{\mathbf{u}}_h. \quad (4)$$

The approximate solution $\hat{\mathbf{u}}_h$ will not satisfy Eq. (3) exactly. The failure is the residual or defect

$$\mathbf{r}_h = \mathbf{f}_h - \mathbf{L}_h \hat{\mathbf{u}}_h. \quad (5)$$

Using Eqs. (4) and (5), the fine grid Eq. (3) is replaced by

$$\mathbf{L}_h(\hat{\mathbf{u}}_h + \mathbf{e}_h) - \mathbf{L}_h \hat{\mathbf{u}}_h = \mathbf{r}_h. \quad (6)$$

The right-hand side is smooth after a few nonlinear relaxation sweeps. Then we can transfer the above equation to a coarse grid:

$$\mathbf{L}_H(\mathbf{u}_H) - \mathbf{L}_H(I_h^H \hat{\mathbf{u}}_h) = I_h^H \mathbf{r}_h, \quad (7)$$

where I_h^H is some restriction operator which transfers variables or residues from the fine grid to the coarse grid. Let $\hat{\mathbf{u}}_H$ denote the approximation solution to Eq. (7). Then the coarse-grid correction is

$$\hat{\mathbf{e}}_H = \hat{\mathbf{u}}_H - I_h^H \hat{\mathbf{u}}_h,$$

Finally, the coarse-grid correction is transferred back to the fine grid to obtain the improved fine grid approximation

$$\hat{\mathbf{u}}_h \leftarrow \hat{\mathbf{u}}_h + I_H^h(\hat{\mathbf{u}}_H - I_h^H \hat{\mathbf{u}}_h),$$

where I_H^h is an interpolation operator which transfers the correction from the coarse grid to the fine grid. The above procedure can be applied recursively to form a complete multigrid V-cycle [14].

4. Stopping criterion

An essential problem of all iteration processes is when to stop the process. A loose stopping criterion generates useless solutions. On the other hand, a too strict stopping criterion results in an inefficient process. One benefit of the multigrid method is that it provides a natural and optimal stopping criterion. In order to understand this stopping criterion, we analyze the errors introduced by the numerical process first.

Rewrite the generalized Reynolds equation as

$$\mathcal{L}(u) = f, \quad (8)$$

where \mathcal{L} stands for the differential operator, u the exact differential solution, and f the source term. The aim is to have a solution of Eq. (8). But it is only possible to compute an approximate solution $\hat{\mathbf{u}}_h$ to the discretized Eq. (3). Let I^h be a projection operator transferring the continuous solution into the discrete function space. The final total error can be expressed as

$$\hat{\mathbf{e}}_h = I^h u - \hat{\mathbf{u}}_h = (I^h u - \mathbf{u}_h) + (\mathbf{u}_h - \hat{\mathbf{u}}_h),$$

where \mathbf{u}_h is the exact solution of Eq. (3). The above equation shows that the total error is composed of the global (discretization) error $\mathbf{e}_h = I^h u - \mathbf{u}_h$, introduced by the discretization process, and of the algebraic error $\mathbf{u}_h - \hat{\mathbf{u}}_h$, caused by the numerical solution of the discrete equation. It is appropriate to require the maximum total error norm of magnitude ε :

$$\|\hat{\mathbf{e}}_h\| \leq \|I^h u - \mathbf{u}_h\| + \|\mathbf{u}_h - \hat{\mathbf{u}}_h\| < \varepsilon. \quad (9)$$

This condition is satisfied if $\|I^h u - \mathbf{u}_h\| < \varepsilon/2$ and $\|\mathbf{u}_h - \hat{\mathbf{u}}_h\| < \varepsilon/2$ independently. The first condition determines the mesh size of the finest grid. The second condition implies that it is sufficient to solve the discrete problem up to the level of global error. Therefore, a natural stopping criterion for a multigrid iteration is

$$\|\mathbf{u}_h - \hat{\mathbf{u}}_h\| \leq \|I^h u - \mathbf{u}_h\|.$$

Since the exact discrete solution \mathbf{u}_h is unknown in general, the residual or defect \mathbf{r}_h as defined by Eq. (5) is employed instead to estimate the algebraic error. In this case, the stopping criterion may be expressed

$$\|\mathbf{r}_h\| \leq c \cdot \|I^h u - \mathbf{u}_h\|, \quad (10)$$

where c is a suitable parameter. Because an analytic representation of the global (discretization) error is impossible in general, another indicator for identifying how well the discrete problem approximates the differential problem is required. Here, the local error as defined by

$$\tau_h = \mathbf{L}_h(I^h u) - \mathbf{f}_h$$

is used. The global error \mathbf{e}_h and local error τ_h are related

by

$$\mathbf{L}_h(\mathbf{u}_h + \mathbf{e}_h) = \mathbf{f}_h + \tau_h.$$

That means, the discrete solution of the discrete problem, where the right-hand side is modified by adding the local error, coincides with the corresponding projection of the differential solution $I^h u$. One benefit of the FAS algorithm is that it offers a numerically cheap possibility to estimate the local error with the aid of two consecutive grids. Define the relative truncation error τ_H^h by

$$\tau_H^h = \mathbf{L}_H(I_H^H \mathbf{u}_h) - I_H^H \mathbf{L}_h(\mathbf{u}_h). \tag{11}$$

This quantity stands for the error that is caused by the substitution of \mathbf{u}_h restricted to the coarse grid into the coarse-grid equation. Since $\mathbf{L}_h(\mathbf{u}_h) = \mathbf{f}_h$, Eq. (11) can be rewritten as

$$\tau_H^h = \mathbf{L}_H(I_H^H \mathbf{u}_h) - \mathbf{f}_H. \tag{12}$$

The local error τ_H on the coarse grid may be considered composed of the local error τ_h on the fine grid and the relative truncation error on the coarse grid with respect to the fine grid:

$$\tau_H = I_h^H \tau_h + \tau_H^h.$$

Assuming the existence of asymptotic expansion for the local error, it is easy to show that [16]

$$\tau_H^h = \frac{H^p - h^p}{H^p} \tau_H. \tag{13}$$

Thus, the relative truncation error τ_H^h equals the local error on the coarse grid, up to higher order terms and a factor depending on the mesh size ratio and the order of consistency. It follows that the local truncation error may be used as an indicator of the local error. For a standard coarse mesh size, $H = 2h$, Eq. (13) can be rewritten as

$$\tau_H = \frac{2^p}{2^p - 1} \tau_H^h$$

Since the exact discrete solution \mathbf{u}_h is unknown, we cannot exactly compute the local truncation error. But we can have an approximation to it from using $\hat{\mathbf{u}}_h$ in Eq. (12):

$$\tau_H^h \approx \hat{\tau}_H^h = \mathbf{L}_H(I_H^H \hat{\mathbf{u}}_h) - \mathbf{f}_H.$$

Using this relation, the stopping criterion (10) may be expressed as

$$\|\mathbf{r}_h\| \leq c \cdot \frac{2^p}{2^p - 1} \|\hat{\tau}_H^h\|. \tag{14}$$

5. Local grid refinement

As discussed in the previous section, the total error is composed of the global (discretization) error and the algebraic error. Eq. (9) is satisfied if both the global and algebraic errors are less than a predetermined tolerance. Therefore, it is sufficient to solve the discrete problem on the finest grid with the goal that the algebraic error is at the level of the global error. The global error is a function of the mesh size. Let $\varepsilon_h(P)$ be the global error estimator at node P of the grid with mesh size h . Then the mesh size h of the finest grid is chosen to guarantee that

$$\varepsilon_h(P) < \text{Tol}, \tag{15}$$

where Tol represents the predetermined tolerance. This condition implies that local refinement is required at nodes where the above relation is violated. In this way, finer grids may be confined to increasingly small domain, so as to provide higher resolution only where needed. The procedure for constructing the finer grid is described below.

Let G_l be the currently finest grid with mesh size $h_l = h_0/2^l$ and $P = (x_p, y_p)$ a node of G_l . If the global error estimator at node P is larger than the predetermined tolerance, a grid patch

$$E_{l+1}(P) = \{Q | Q = (x_p + \alpha h_{l+1}, y_p + \alpha h_{l+1}), \quad |\alpha| \leq 2\}$$

is introduced on the next finer grid G_{l+1} with mesh size $h_{l+1} = h_l/2$. In the sequel, this is referred to as the elementary refinement patch. The complete grid G_{l+1} is obtained by the union of all elementary refinement patches introduced over all G_l nodes, where a better grid resolution is required. Fig. 2 shows a typical two-grid adaptive structure. The finer grid G_{l+1} consists of three elementary patches introduced over nodes P_1 , P_2 , and P_3 of G_l , respectively. Note that the finer grid G_{l+1} is disconnected and only covers part of the entire

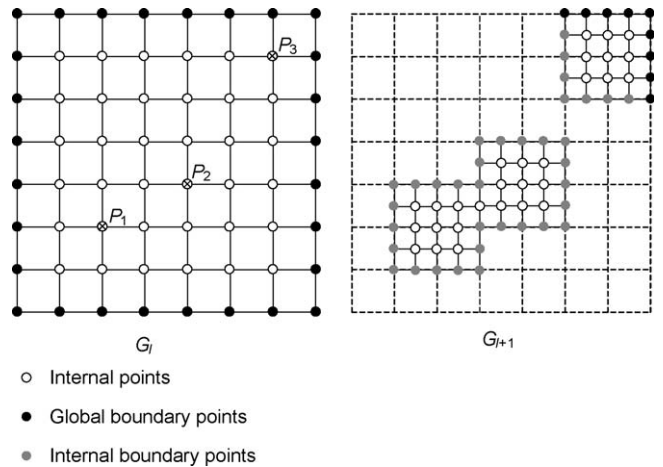


Fig. 2. A typical two-grid adaptive structure.

domain. A grid that covers the whole domain is called a global grid. Otherwise, it is local.

The above refinement process can be applied repeatedly until the requirement on the discretization error is satisfied all over the finest grid. Then the final multi-level adaptive grid structure is a set of uniform grid

$$G = \{G_1, G_2, \dots, G_M\},$$

where G_l refers to the uniform grid that covers the domain Ω_l on the l th level. The mesh size of G_l is $h_l = h_1/2^{l-1}$. On the first m_g ($1 \leq m_g \leq M$) levels the grids are global, while the other uniform grids on level $l > m_g$ are local ones defined on subdomains for which $\Omega_l \subset \Omega_{l-1}$ holds. M denotes the finest level. By using properly aligned elementary patches to construct uniform local grids on different levels, the globally required non-uniform resolution of the discrete approximation can be obtained. This leads to important simplifications both for the discretization and for the handling of the adaptive grid structure.

6. FAS on composite grid

Note that the final multilevel grid structure may be composed of grids with different domains. In other words, some nodes of G_{l-1} may not belong to the next finer grid G_l . Therefore, some modifications on the FAS algorithm, which works well on global grids, are required before we can apply it on local grids. The modified FAS scheme is described briefly on a two-level grid structure. Let G_h and G_H denote two consecutive grids, and G_h^0 and G_H^0 the corresponding sets of interior points of G_h and G_H , respectively (see Fig. 2). For a refinement local grid G_h , some of the boundary points, $G_h - G_h^0$, are internal boundary points (gray solid points in Fig. 2). At these points, function values should be interpolated properly from the corresponding points on G_H . The discrete equation together with the boundary conditions can be expressed as

$$\mathbf{L}_h \mathbf{u}_h = \mathbf{f}_h \text{ on } G_h^0$$

and

$$\mathbf{u}_h = \mathbf{I}_H^h \mathbf{u}_H \text{ on } G_h - G_h^0.$$

For those interior points of G_H which do not belong to G_h^0 , G_H is the finest discretization level. A solution to the discrete problem has to be computed there. On the other hand, the interior points of G_H which are also interior points of G_h are used to calculate corrections to the approximate solution on G_h^0 . By defining

$$\mathbf{F}_H = \begin{cases} \mathbf{L}_H \mathbf{I}_h^H \mathbf{u}_h & \text{on } G_H^0 \cap G_h^0 \\ \mathbf{f}_H & \text{on } G_H^0 - (G_H^0 \cap G_h^0), \end{cases}$$

the discrete problem on the coarse grid can be expressed in a compact form as (compared with Eq. (7))

$$\mathbf{L}_H \mathbf{u}_H = \mathbf{F}_H.$$

This modified two-grid FAS scheme can be applied recursively as before to form a complete V-cycle multi-grid scheme.

7. Adaptive multilevel method

The grid refinement process and the solution algorithm as described above are combined together to form the complete adaptive multilevel method. Fig. 3 shows the flow chart of this method. In this method, the global errors on the entire domain are controlled adaptively to be under a predetermined tolerance. The

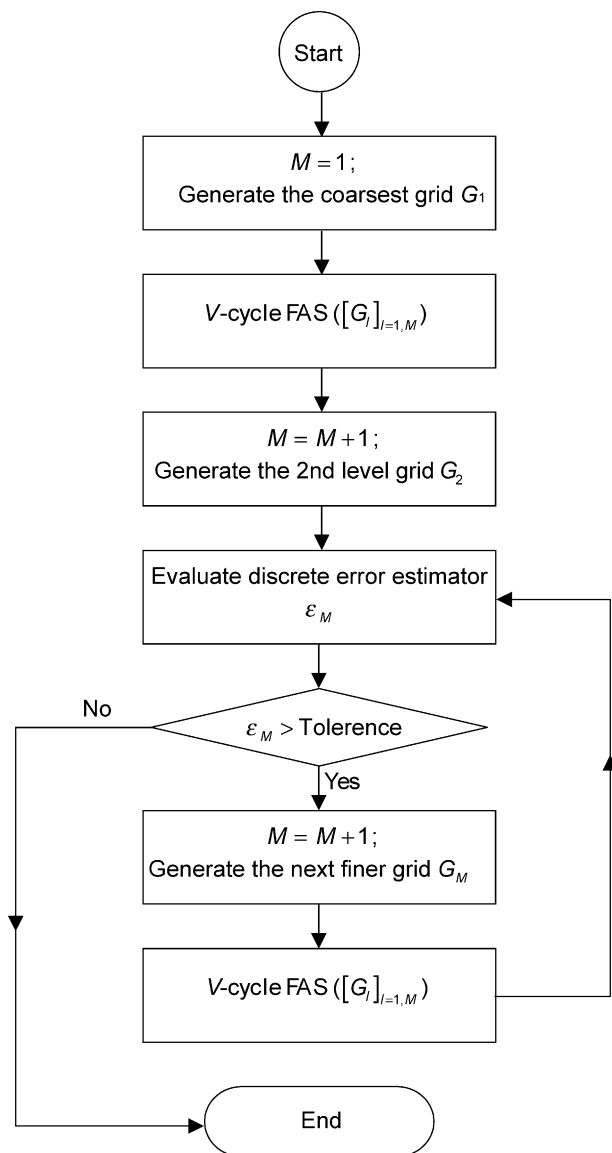


Fig. 3. Flow chart of the adaptive multilevel method.

essential phase of the adaptive control of global errors is their evaluation for the given discrete problem. Here, the τ -extrapolation of the relative truncation error on two consecutive grids is employed as the discretization error estimator [12]. Therefore, two global grids G_1 and G_2 are required to initialize the adaptive process. The complete algorithm is described briefly below. Let G_M ($M \geq 2$) denote the currently finest grid. The initial guess on G_M is obtained by interpolating from the next coarser grid G_{M-1} . Then the V-cycle FAS algorithm is applied repeatedly until the algebraic error on the currently finest grid is less than the discretization error. After that, new refinement is constructed over the currently finest grid where the discretization error exceeds the predetermined tolerance. These steps are recursively repeated until no further refinement is needed.

8. Results and discussion

The static pressure of a 30% tri-rail slider [17] is calculated using the multilevel numerical scheme developed in this paper. The flying height is 15 nm, the pitch angle is 180 μ rad, the sliding velocities in the x - and y -directions are 13.47 and 16.28 m/s, respectively. Fig. 4 illustrates the air-bearing surface of the 30% tri-rail slider. This slider has a center rail that carries the read-write element. The connected front region enables the efficient generation of the sub-ambient pressure in the central recessed regions. The rail has concave shapes on both sides to minimize the flying height change across the disk. Fig. 5(a) shows the 3-D pressure distribution over the entire slider. Along

the outer shaped rails, the air is pressurized due to the wedge effect provides by the front taper and flat step. Over the central portion of the slider, the flow expands rapidly across the step discontinuity and hence generates sub-ambient pressure. In order to see the sub-ambient pressure clearly, the pressure profile along the line $y/L = 0.3$ is shown in Fig. 5(b). On the front taper and flat step, the pressure rises to the maximum value of about 1.4 and drops right down to 0.36 passing the flat step. In the front recessed region, the pressure increases due to the convergent cross-section. The pressure has a steep rise on the shaped rail and another rapid drop crossing the shaped rail. Then it increases monotonically to the ambient pressure. Note that the pressure gradient in the center recessed region is higher than that on the front taper and flat step.

Figs. 6(a) and (b) show the composite grids at the fourth and fifth level, respectively. From these two figures, it can be seen that the regions with sudden geometric change or high pressure gradient have been efficiently covered by fine meshes generated by the adaptation scheme. Almost all the center recessed regions are refined at the fifth level due to the large pressure variations as shown in Fig. 5(b). Local refinements and the composite grid structure can be seen clearly from Figs. 6(a) and (b).

In order to see the effects of the mesh size on the numerical results, the normal force obtained at each level of grid is plotted in Fig. 7, where Tol stands for the refinement criterion. The coarsest grid consists of 31×31 nodes. Smaller values of Tol indicate that more elementary refinement patches are introduced at each

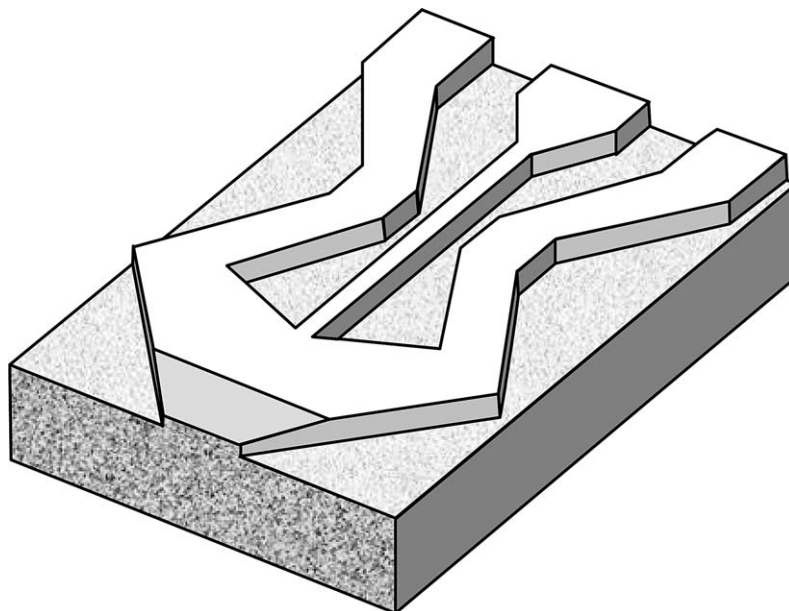


Fig. 4. Schematic of the 30% tri-rail slider.

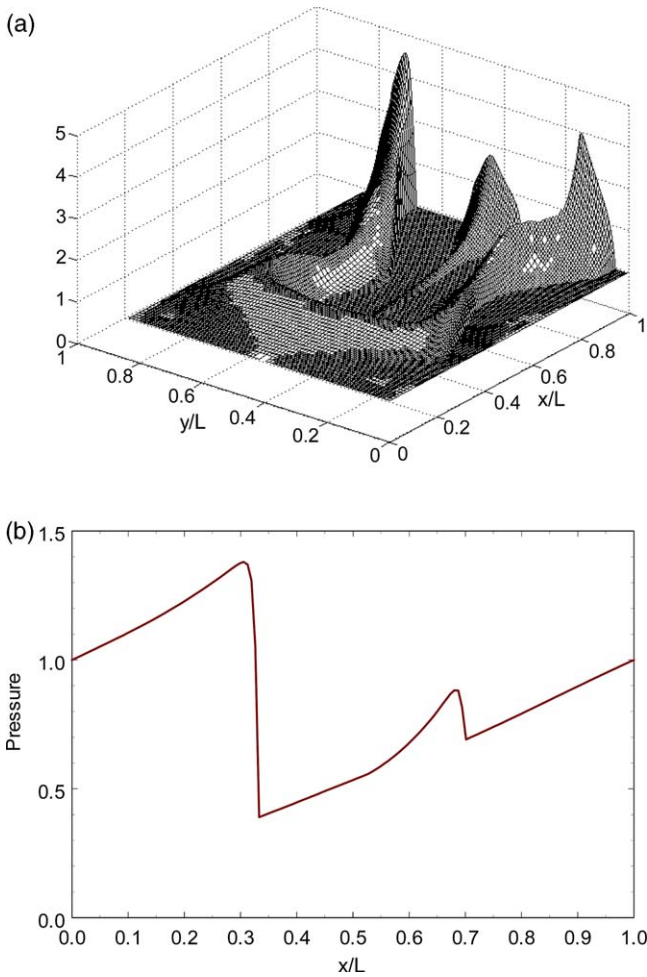


Fig. 5. Pressure distribution of the 30% tri-rail slider: (a) 3-D pressure profile at the fourth level over the entire slider, and (b) pressure profile along the line $y/L = 0.3$.

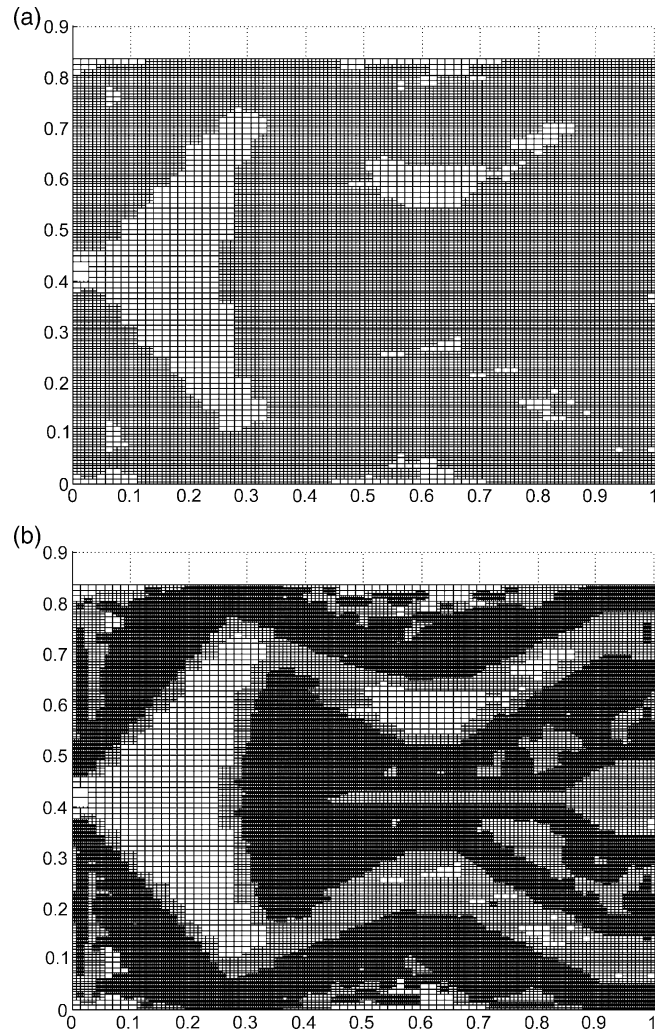


Fig. 6. Composite grids at (a) the fourth level and (b) the fifth level.

level. As can be seen from the figure, the normal force converges as the number of levels increases for each value of Tol. The results for Tol = 20 and 30 are almost identical. Hence, it can be concluded that the grid structure to the 8th level for Tol = 30 is appropriate for describing the pressure distribution under the slider.

Fig. 8 shows the total number of nodes up to the current finest grid for Tol = 0 and 30. Tol = 0 indicates that uniform global grid is used at each level. In this case, the node number increases exponentially with the level number. As can be seen from the figure, the node number for Tol = 30 is much less than that for Tol = 0. The total number of nodes up to the 8th level for Tol = 30 is about 1/20 of that for Tol = 0. This shows that the proposed adaptive multilevel method is significantly more efficient than the non-adaptive multigrid method since the computation work increases rapidly with the node number.

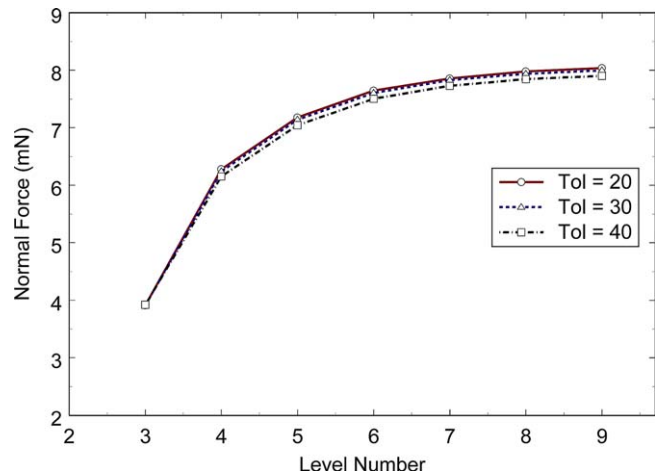


Fig. 7. Normal force versus level number for various refinement criteria.

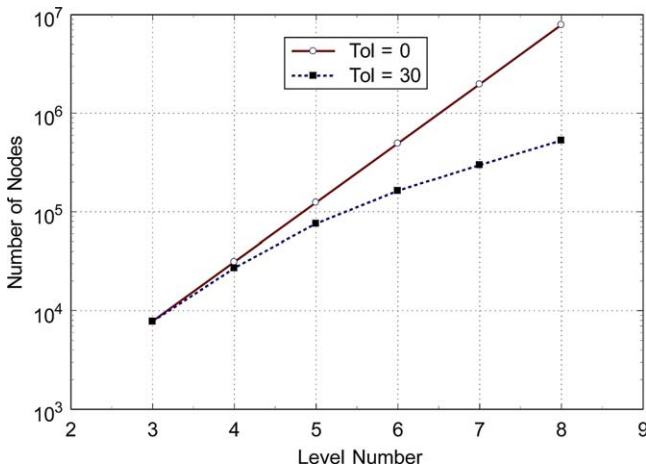


Fig. 8. Number of nodes up to the finest grid for Tol = 0 and 30.

9. Conclusions

Due to the complicated air-bearing surface of slider in hard disk drives, efficient numerical methods are required for analyzing the pressure distribution under the slider. The usual approach is first to discretize the generalized Reynolds equation in some preassigned manner, and then to submit the resulting discrete equations to some numerical solution process. In this study, the discretization and solution processes are combined together, and greatly benefit from each other. An adaptive grid-generating scheme is implanted to discretize the computation domain. The final grid system consists of a sequence of uniform grids (or levels) with decreasing mesh sizes. The domain of any grid may be only a proper part of the domains of the coarse grids. This structure is very flexible and allows an efficient handling of the refinement. The FAS algorithm, which suits well for solving nonlinear equations, is used to obtain solutions on these levels of grids. The grid adaptation is governed by the relative truncation errors supplied by the FAS algorithm, and can naturally be integrated with the FAS algorithm to give high resolution where needed. Calculations on a 30% tri-rail slider show that this multilevel FAS method is much more efficient than the traditional multigrid method using uniform global grids.

Acknowledgements

This research was supported by the National Science Council of the Republic of China under Grant No. NSC-89-2212-E-002-109.

References

- [1] White JW. Flying characteristics of the zero-load slider bearing. *Journal of Lubrication Technology* 1983;105:484–90.
- [2] Harde C, Menon A, Crane P, Egbert D. Analysis and performance characteristics of the Seagate advanced air bearing slider. *IEEE Transactions on Magnetics* 1994;30(2):424–32.
- [3] White JW. Flying characteristics of the transverse and negative pressure contour (“TNP”) slider air bearing. *ASME Journal of Tribology* 1997;119:241–9.
- [4] Tang T. Dynamics of air-lubricated slider bearings for non-contact magnetic recording. *ASME Journal of Lubrication Technology* 1971;93:272–8.
- [5] White JW, Nigam A. A factored implicit scheme for the numerical solution of the Reynolds equation at very low spacing. *ASME Journal of Lubrication Technology* 1980;102:80–4.
- [6] Ruiz OJ, Bogy DB. A numerical simulation of the head-disk assembly in magnetic hard disk: 1. Component models. *ASME Journal of Tribology* 1990;112:593–602.
- [7] Wahl MH, Lee PR, Talke FE. An efficient finite element-based air bearing simulator for pivoted slider bearings using bi-conjugate gradient algorithms. *Tribology Transactions* 1996;39(1): 130–138.
- [8] Cha E, Bogy DB. A numerical scheme for static and dynamic simulation of subambient pressure shaped rail sliders. *ASME Journal of Tribology* 1995;117:36–46.
- [9] Hu Y. Head-disk-suspension dynamics. Doctoral Dissertation, Department of Mechanical Engineering, University of California, Berkeley, 1996.
- [10] Lu S. Numerical simulation of slider air bearings. Doctoral Dissertation, Department of Mechanical Engineering, University of California, Berkeley, 1997.
- [11] Wu L, Bogy DB. Unstructured adaptive triangular mesh generation techniques and finite volume schemes for the air bearing problem in hard disk drives. *ASME Journal of Tribology* 2000;122:761–70.
- [12] Brandt A. Multilevel adaptive solutions to boundary-value problems. *Mathematics of Computation* 1977;31(138):333–90.
- [13] Hackbusch W, Trottenberg U, editors. *Multigrid methods*. Springer-Verlag; 1982.
- [14] Briggs WL. *A multigrid tutorial*. Philadelphia (PA): Society for Industrial and Applied Mathematics; 1987.
- [15] Patankar SV. *Numerical heat transfer and fluid flow*. New York: McGraw-Hill; 1980.
- [16] Joppich W, Mijalkovic S. *Multigrid methods for process simulation*. New York: Springer-Verlag; 1993.
- [17] Kang TS, Choi DH, Jeong TG. Optimal design of HDD air-lubricated slider bearings for improving dynamic characteristics and operating performance. *ASME Journal of Tribology* 2001;123:541–7.